Imaging Biomarker Development for Detection of Hepatocellular Carcinoma

David Fuentes

The University of Texas MD Anderson Cancer Center

Biomedical Systems Engineering - Advanced Techniques for Biomedical Signal and Image Processing and Device Modeling
October 28, 2024

Background

- Screening programs for patients with cirrhosis are well established and have been demonstrated to improved survival outcomes through early detection of HCC

- However, there are currently limited methods to risk-stratify patients or quantitatively characterize small liver lesions, measuring less than 2cm in diameter, in screened populations.

- **Hypothesis**: Quantitative imaging signal of the background parenchyma, with or without small liver lesions present, characterizes a patient's risk of developing HCC.

What do we do with indeterminate lesions?

Journal of Hepatocellular Carcinoma

Dovepress
open access to scientific and medical research

Open Access Full Text Article

ORIGINAL RESEARCH

Enhancement Pattern Mapping for Early Detection of Hepatocellular Carcinoma in Patients with Cirrhosis

Newsha Nikzad[1–3,*], David Thomas Fuentes[4,*], Millicent R
Matthew Cagley[2], Mohamed Badawy[4], Ahmed Elkhesen[5], M
Laura Beretta[8], Eugene Jon Koay[2], Prasun Kumar Jalal[1]

[1]Department of Medicine and Surgery, Baylor College of Medicine, Houston, TX, USA; [2]D
MD Anderson Cancer Center, Houston, TX, USA; [3]Department of Internal Medicine, Th
[4]Department of Imaging Physics, The University of Texas MD Anderson Cancer Center, H
Tech University Health Sciences Center, Lubbock, TX, USA; [6]Department of Epidemiolog
Houston, TX, USA; [7]Department of Abdominal Imaging, The University of Texas MD And
Molecular and Cellular Oncology, The University of Texas MD Anderson Cancer Center,

*These authors contributed equally to this work

Correspondence: Newsha Nikzad; Prasun Kumar Jalal, Email nnikzad@bcm.edu; jalal@bc

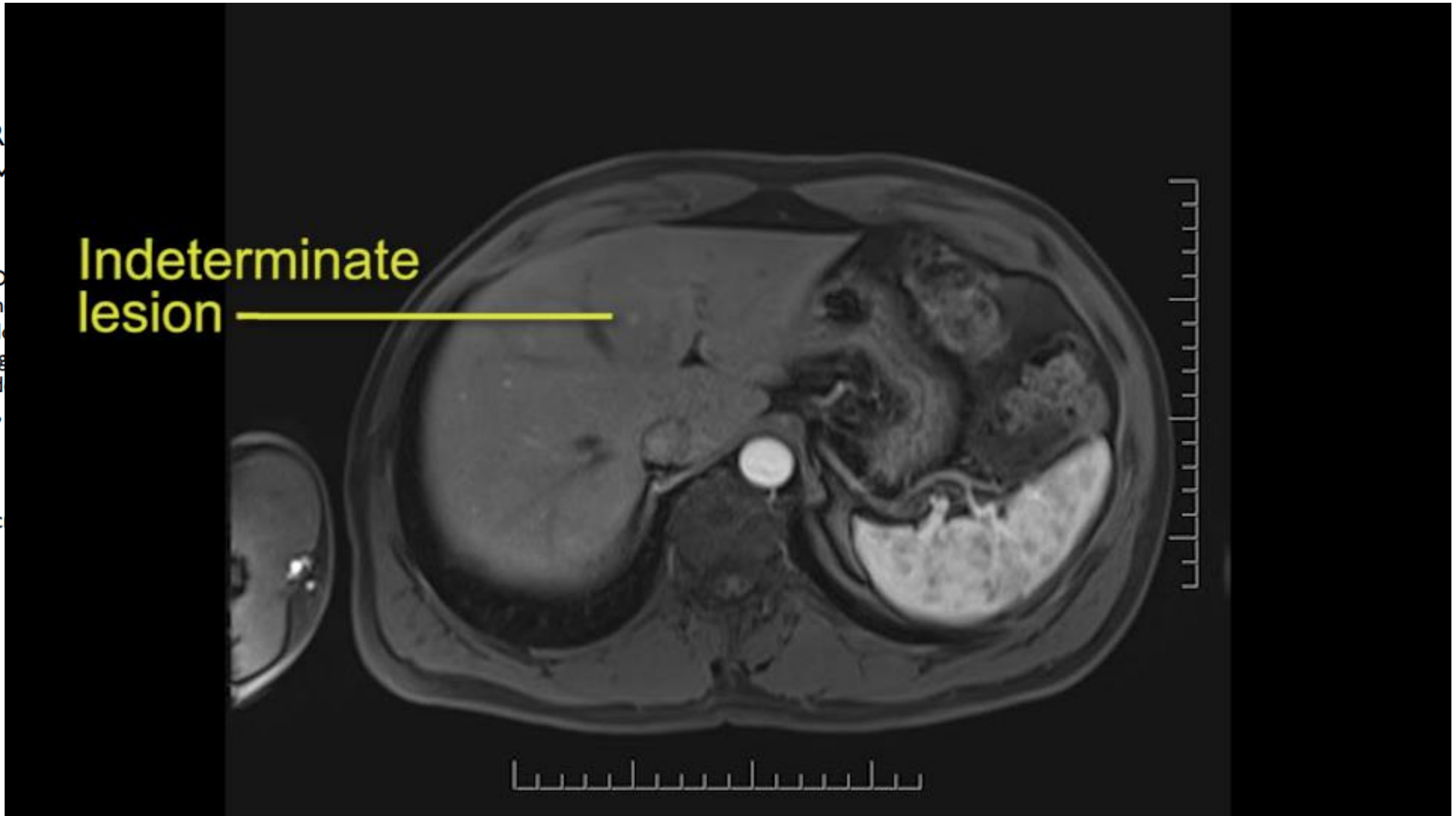

Increasing conspicuity of lesions

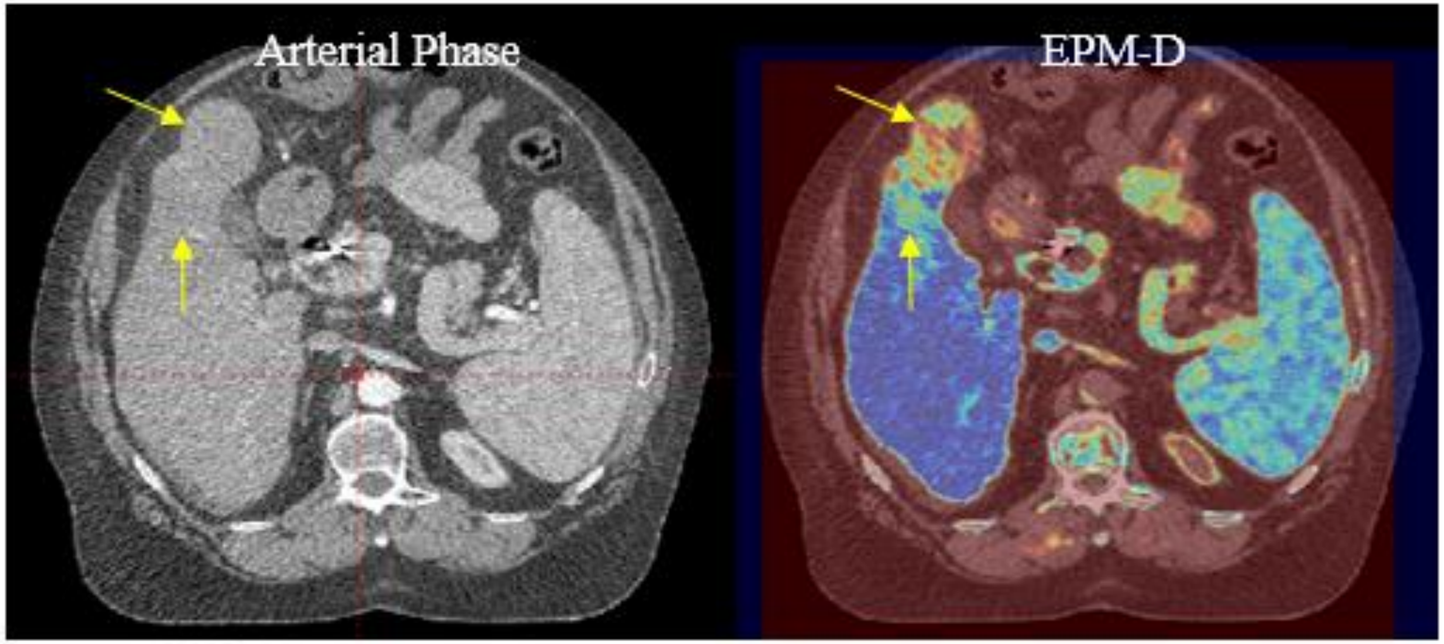

63 y/o male with HCC

Our approach: Maximize standard of care imaging

- Aggregate all the imaging data, enabling a comprehensive assessment
- Apply radiomic and machine learning to these novel signals

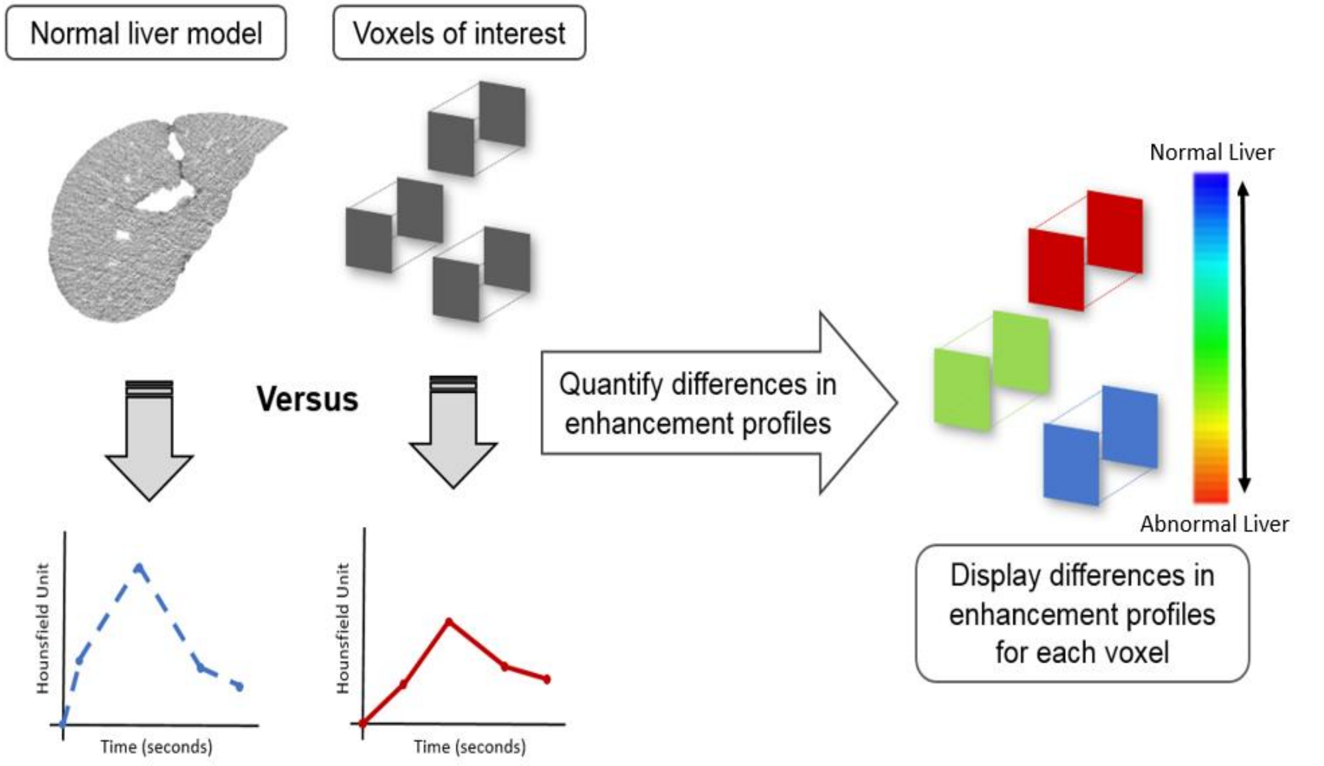

Park et al, Med Phys 2019

Workflow

- Reproducible - Relational database driven workflow
- High throughput - Processing pipeline implemented on HPC cluster for analysis at scale

Liver mask

1.

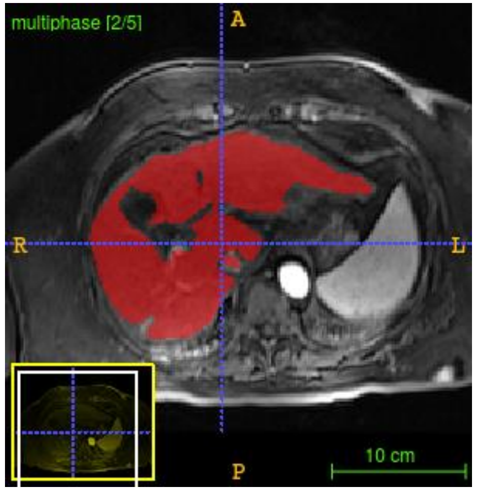

Lesion segmentation

2.

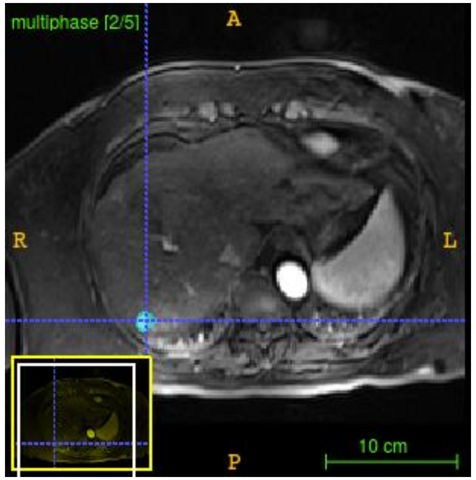

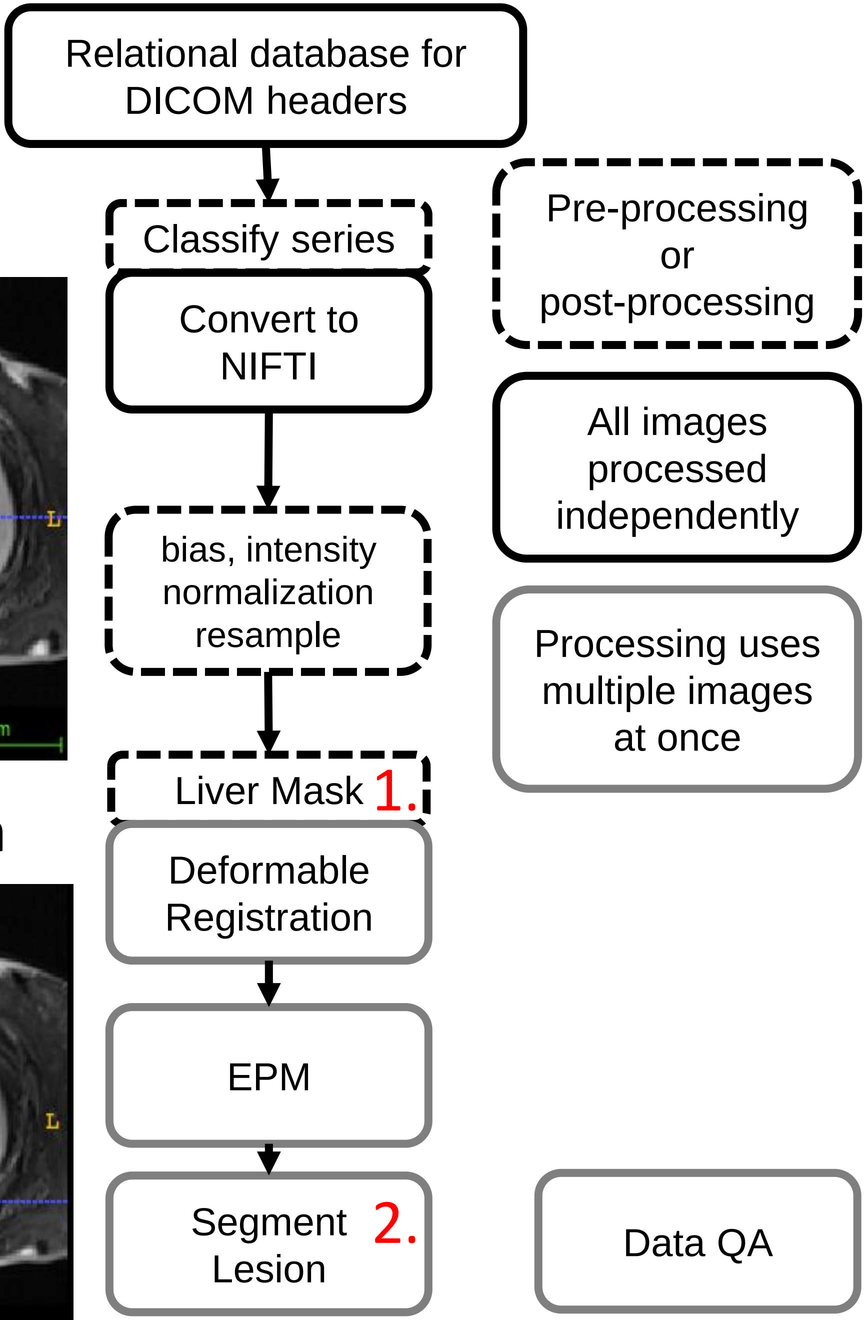

Image series curation

- Build searchable DICOM database with 3d Slicer
  - Local self contained sqlite
- REGEX to identify image series

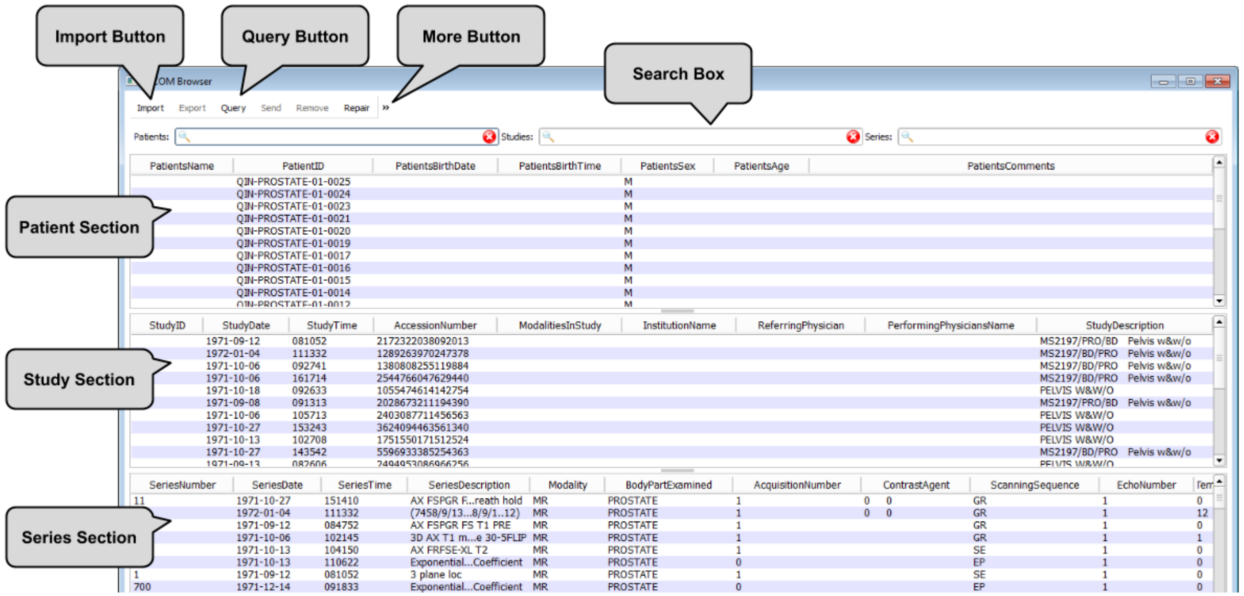

Final image types:

1. T1w liver protocol image
   I. pre-contrast
   II. Arterial phase
   III. Venous phase
   IV. Delay
   V. Post-contrast

MR intensity normalization

- MR images are non-quantitative.
- Scaling based on bias correction, z-score, clipping [-5,5]

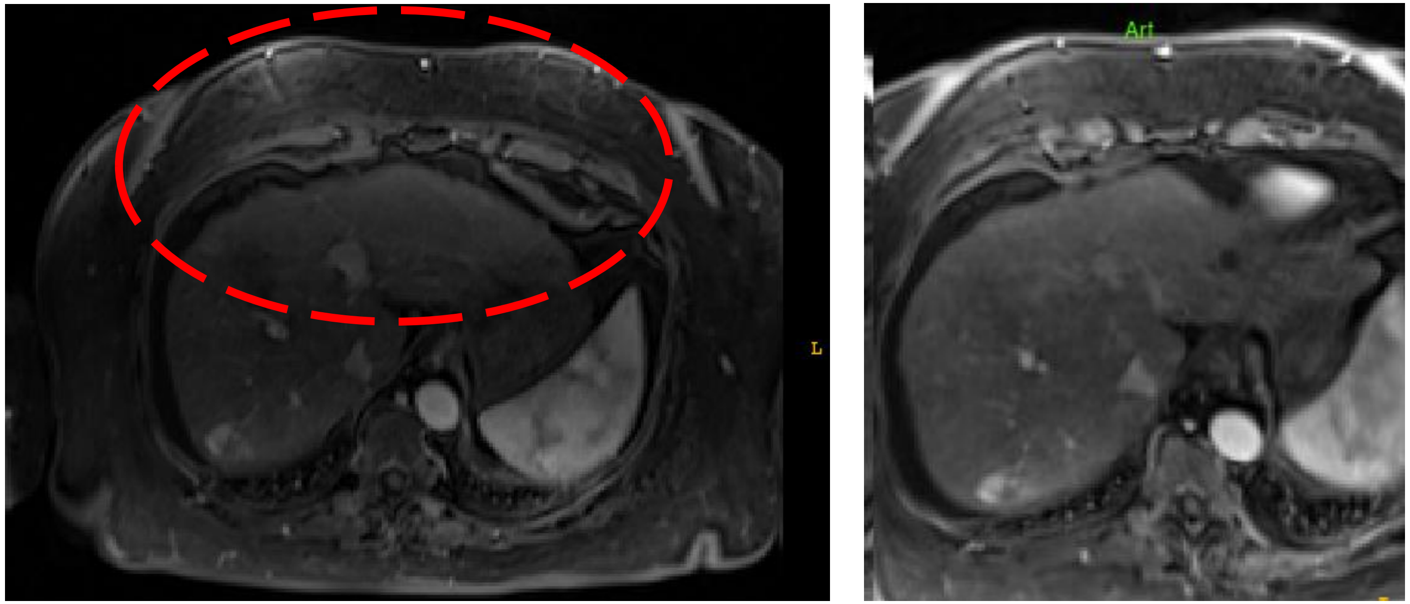

Raw intensity distributions for two patients

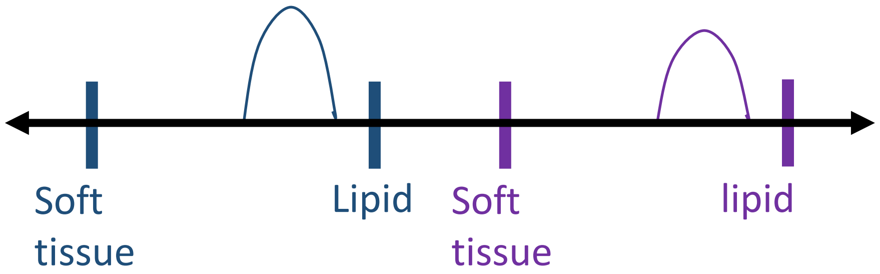

Scaled intensity distributions

$$\frac{x - mean}{std}$$

Image Segmentation

Role of NN is for EPM support:
Segmentation

IEEE TRANSACTIONS ON MEDICAL IMAGING, VOL. XX, NO. XX, XXXX 2021

PocketNet:
Saves time
Saves memory
Preserves performance

PocketNet: A Smaller Neural Network For Medical Image Analysis

Adrian Celaya, Jonas A. Actor, Rajarajesawari Muthusivarajan, Evan Gates, Caroline Chung, Dawid Schellingerhout, Beatrice Riviere, and David Fuentes

https://ieeexplore.ieee.org/document/9964128

Under the hood

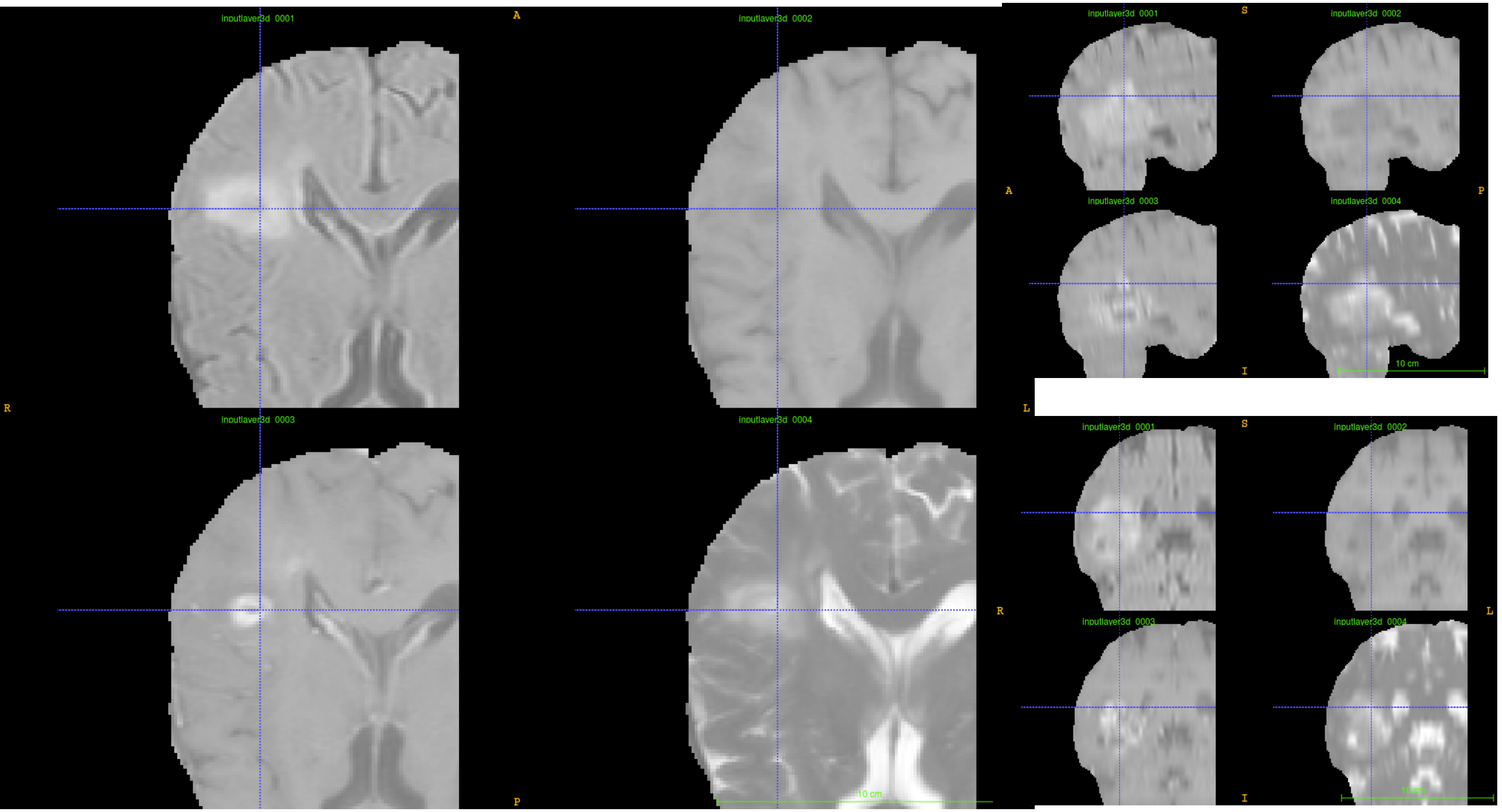

Layer 1 Input Layer

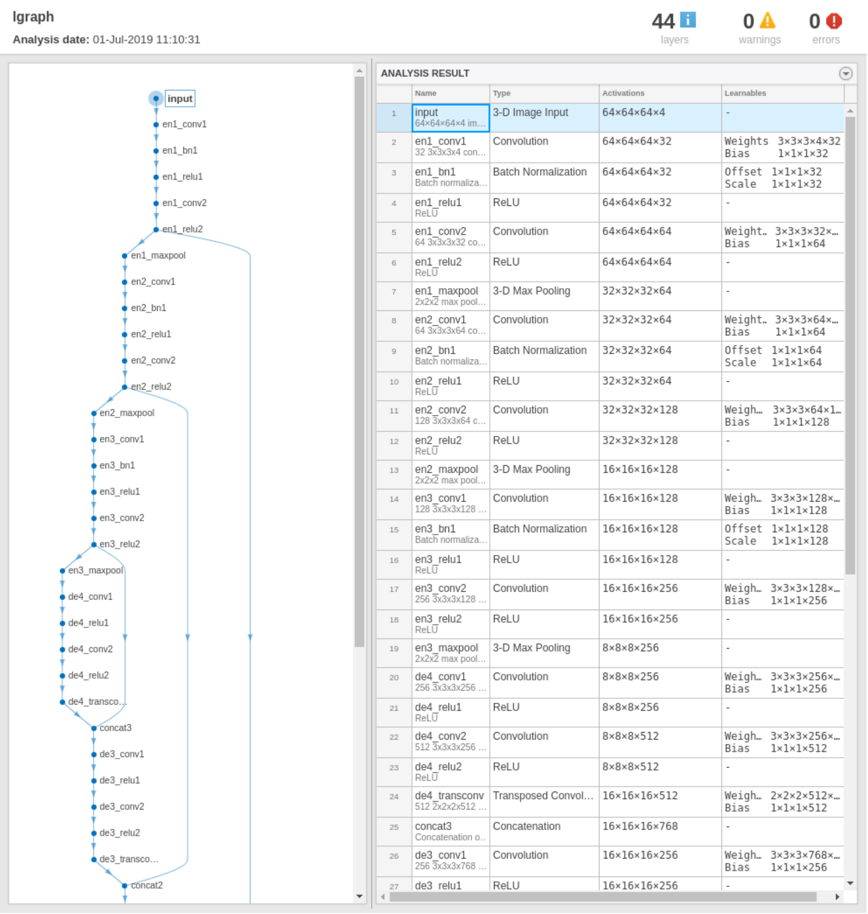

	Name	Type	Activations	Learnables
1	input 64×64×64×4 im...	3-D Image Input	64×64×64×4	-
2	en1_conv1 32 3x3x3x4 con...	Convolution	64×64×64×32	Weights 3×3×3×4×32 Bias 1×1×1×32
3	en1_bn1 Batch normaliza...	Batch Normalization	64×64×64×32	Offset 1×1×1×32 Scale 1×1×1×32
4	en1_relu1 ReLU	ReLU	64×64×64×32	-
5	en1_conv2 64 3x3x3x32 co...	Convolution	64×64×64×64	Weight... 3×3×3×32×... Bias 1×1×1×64
6	en1_relu2 ReLU	ReLU	64×64×64×64	-
7	en1_maxpool 2x2x2 max pool...	3-D Max Pooling	32×32×32×64	-
8	en2_conv1 64 3x3x3x64 co...	Convolution	32×32×32×64	Weight... 3×3×3×64×... Bias 1×1×1×64
9	en2_bn1 Batch normaliza...	Batch Normalization	32×32×32×64	Offset 1×1×1×64 Scale 1×1×1×64
10	en2_relu1 ReLU	ReLU	32×32×32×64	-
11	en2_conv2 128 3x3x3x64 c...	Convolution	32×32×32×128	Weigh... 3×3×3×64×1... Bias 1×1×1×128
12	en2_relu2 ReLU	ReLU	32×32×32×128	-
13	en2_maxpool 2x2x2 max pool...	3-D Max Pooling	16×16×16×128	-
14	en3_conv1 128 3x3x3x128 ...	Convolution	16×16×16×128	Weigh... 3×3×3×128×... Bias 1×1×1×128
15	en3_bn1 Batch normaliza...	Batch Normalization	16×16×16×128	Offset 1×1×1×128 Scale 1×1×1×128
16	en3_relu1 ReLU	ReLU	16×16×16×128	-
17	en3_conv2 256 3x3x3x128 ...	Convolution	16×16×16×256	Weigh... 3×3×3×128×... Bias 1×1×1×256
18	en3_relu2 ReLU	ReLU	16×16×16×256	-
19	en3_maxpool 2x2x2 max pool...	3-D Max Pooling	8×8×8×256	-
20	de4_conv1 256 3x3x3x256 ...	Convolution	8×8×8×256	Weigh... 3×3×3×256×... Bias 1×1×1×256
21	de4_relu1 ReLU	ReLU	8×8×8×256	-
22	de4_conv2 512 3x3x3x256 ...	Convolution	8×8×8×512	Weigh... 3×3×3×256×... Bias 1×1×1×512
23	de4_relu2 ReLU	ReLU	8×8×8×512	-
24	de4_transconv 512 2x2x2x512 ...	Transposed Convol...	16×16×16×512	Weigh... 2×2×2×512×... Bias 1×1×1×512
25	concat3 Concatenation o...	Concatenation	16×16×16×768	-
26	de3_conv1 256 3x3x3x768 ...	Convolution	16×16×16×256	Weigh... 3×3×3×768×... Bias 1×1×1×256
27	de3_relu1	ReLU	16×16×16×256	-

128x128x128x4

Under the hood

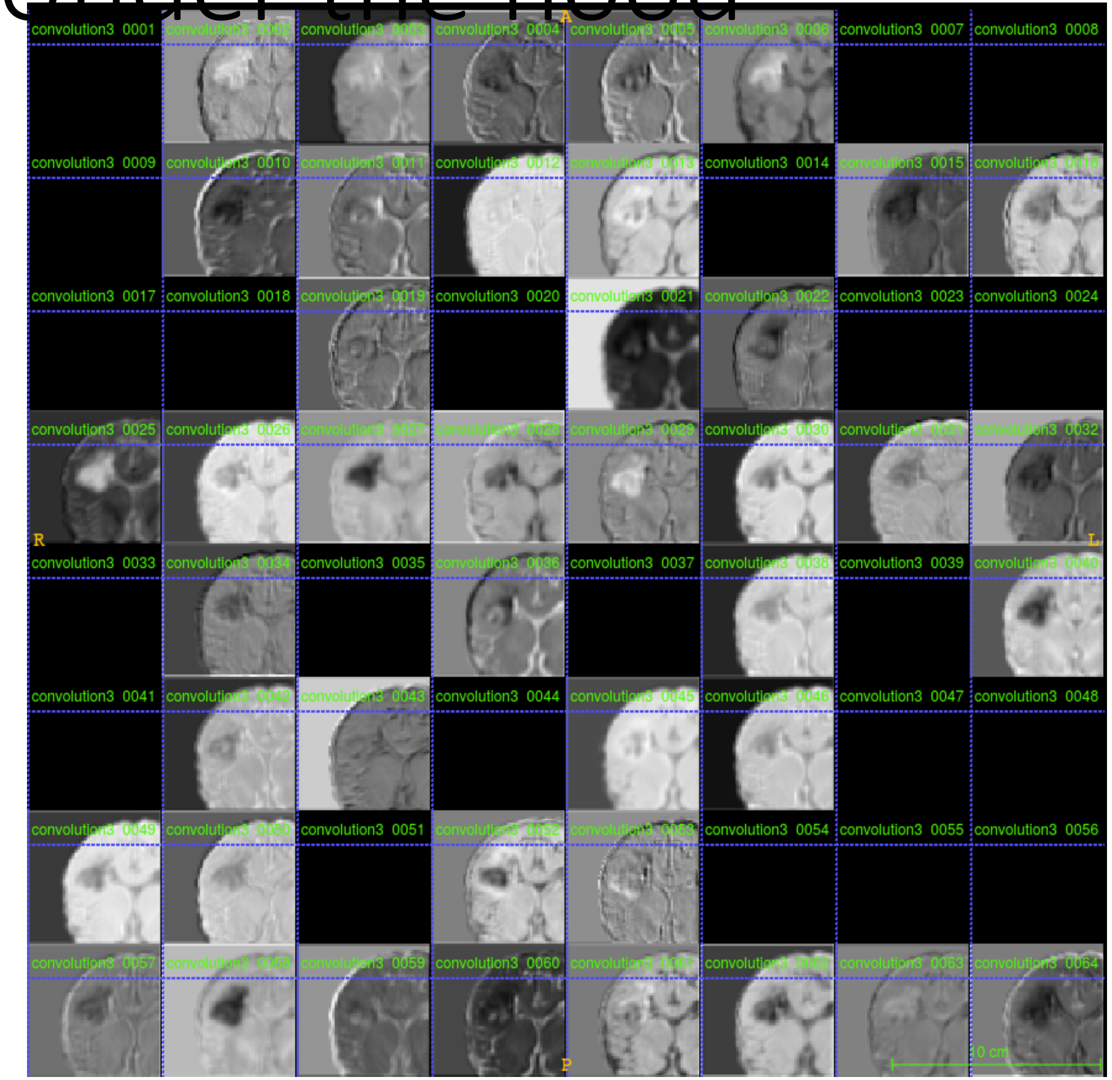

64x64x64x64

Layer 8 Convolution Module 2 Level

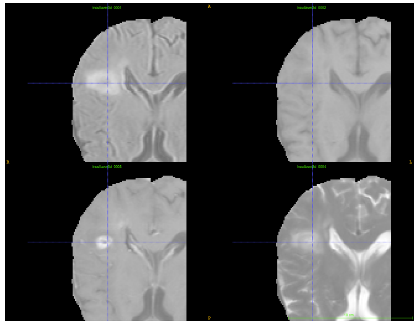

Input Channels

Under the hood

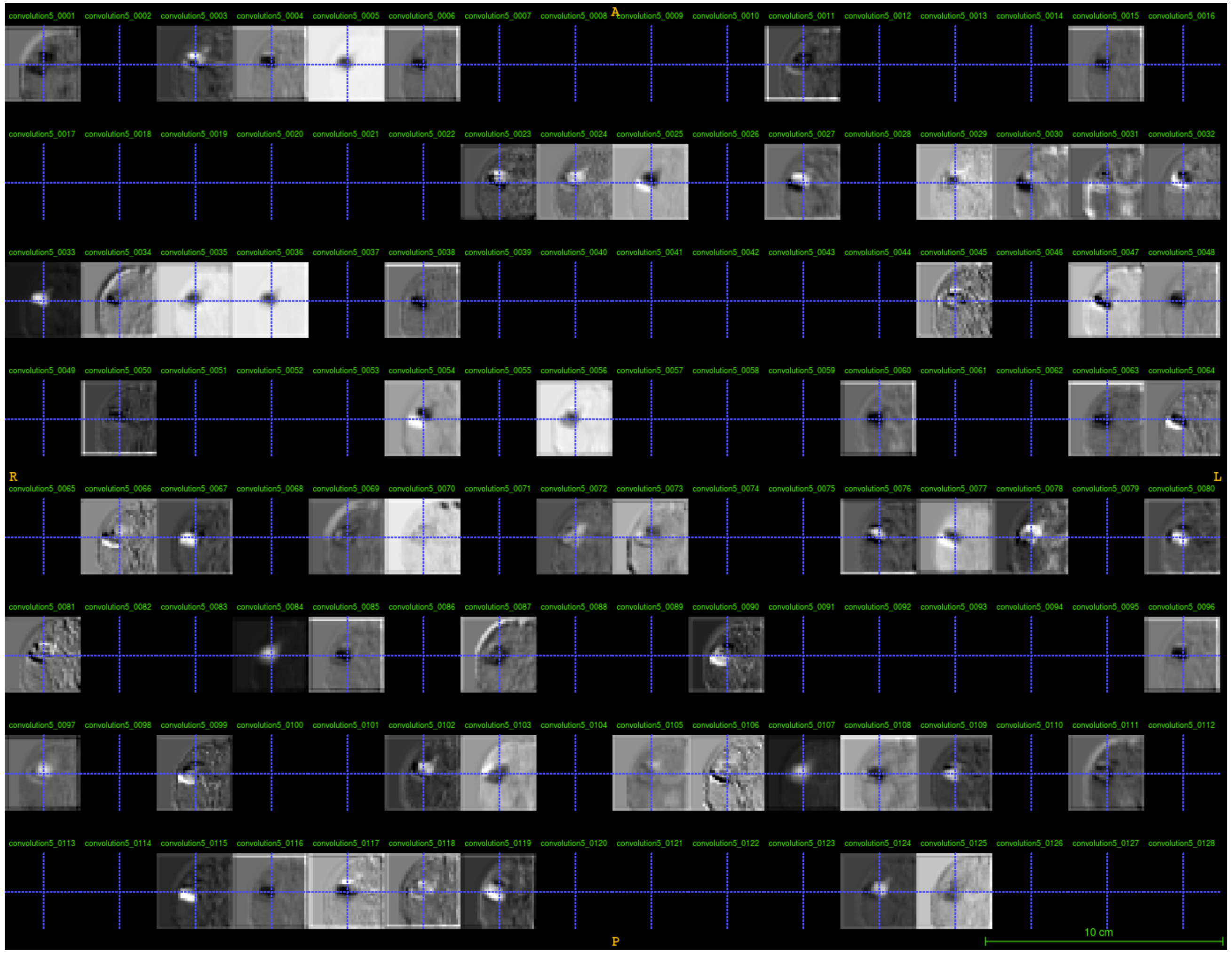

32x32x32x128

Layer 14 Convolution Module 3 Lev

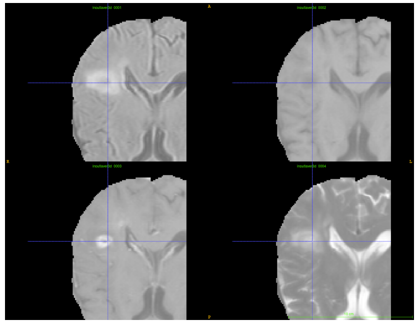

Input Channels

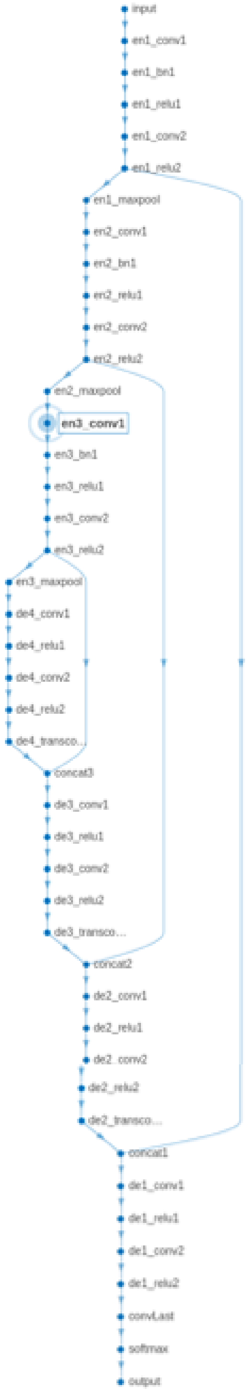

Under the hood

16x16x16x256

Layer 19 Maxpool Module 3

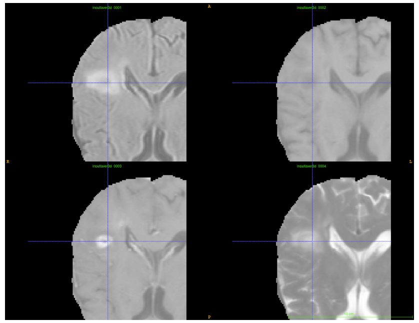

Input Channels

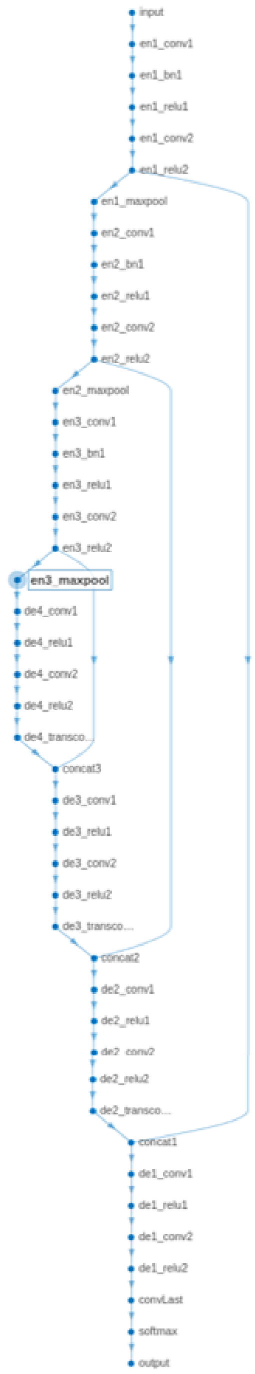

Geometric Multigrid Methods (GMMs)

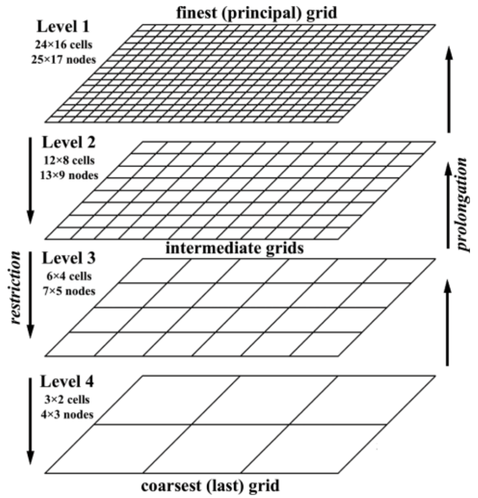

- GMMs are used for solving the linear system
- $$A\,u = f$$
- Matrix A, vector f, and unknown u are related to the geometric grid

- GMMs construct a series of grid at hierarchical resolutions
  - specific frequencies are inherent to each resolution
  - solution is a superposition of the frequencies
  - not necessary to double the number of channels

$$
\begin{aligned}
x_0 &= h^{\otimes}(L_{64\leftarrow 32}\, h^{\otimes}(n^{\otimes}(L_{32\leftarrow 4} I + \vec{b})) + \vec{b}) \\
x_1 &= h^{\otimes}(L_{128\leftarrow 64}\, h^{\otimes}(n^{\otimes}(L_{64\leftarrow 64}\, P\, x_0 + \vec{b})) + \vec{b}) \\
x_2 &= h^{\otimes}(L_{256\leftarrow 128}\, h^{\otimes}(n^{\otimes}(L_{128\leftarrow 128}\, P\, x_1 + \vec{b})) + \vec{b}) \\
x_3 &= h^{\otimes}(L_{512\leftarrow 256}\, h^{\otimes}(L_{256\leftarrow 256}\, P\, x_2 + \vec{b}) + \vec{b}) \\
x_4 &= h^{\otimes}\left(L_{256\leftarrow 256}\, h^{\otimes}\left(L_{256\leftarrow 768} \begin{bmatrix} L^{\top} x_3 + \vec{b} \\ x_2 \end{bmatrix} + \vec{b}\right) + \vec{b}\right) \\
x_5 &= h^{\otimes}\left(L_{128\leftarrow 128}\, h^{\otimes}\left(L_{128\leftarrow 384} \begin{bmatrix} L^{\top} x_4 + \vec{b} \\ x_1 \end{bmatrix} + \vec{b}\right) + \vec{b}\right) \\
x_6 &= h^{\otimes}\left(L_{64\leftarrow 64}\, h^{\otimes}\left(L_{64\leftarrow 192} \begin{bmatrix} L^{\top} x_5 + \vec{b} \\ x_0 \end{bmatrix} + \vec{b}\right) + \vec{b}\right) \\
O &= \phi^{\otimes}(L_{2\leftarrow 64}\, x_6 + \vec{b}) = \phi^{\otimes}\left(\left[\sum_{\alpha} w_1^{\alpha} x_{6\alpha} \quad \dots \quad \sum_{\alpha} w_{N_{\text{class}}}^{\alpha} x_{6\alpha}\right] + \vec{b}\right)
\end{aligned}
$$

Full U-Net

Pocket U-Net

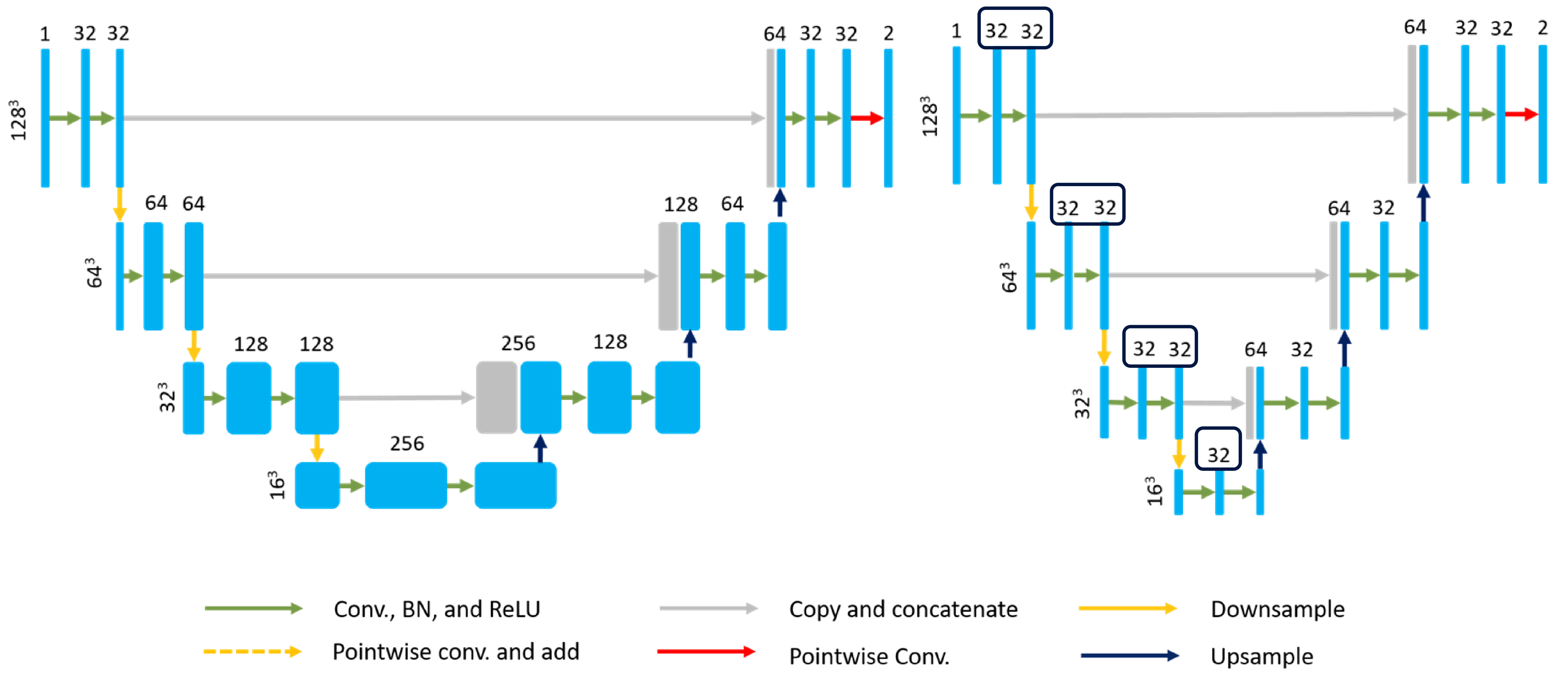

Can we reduce the time and memory required?

Can we preserve accuracy?

Parameter Savings in Practice

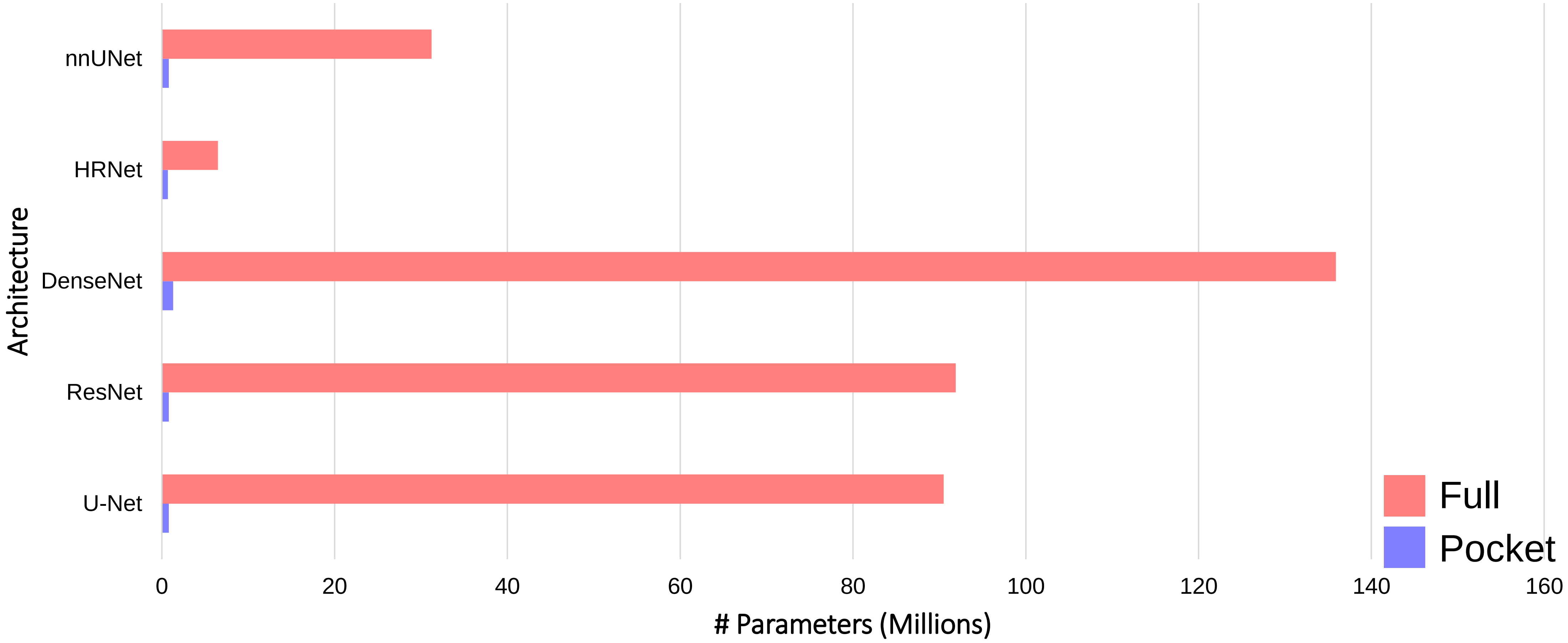

Can we reduce the time and memory required?

Can we preserve accuracy?

Segmentation Tasks – LiTS

131 CT scans of the liver

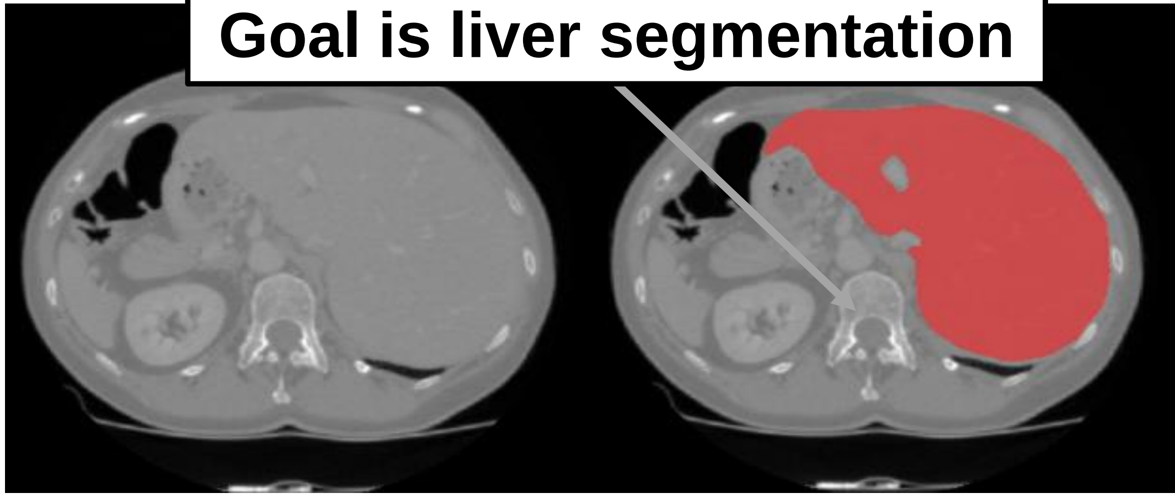

Comparable Accuracy

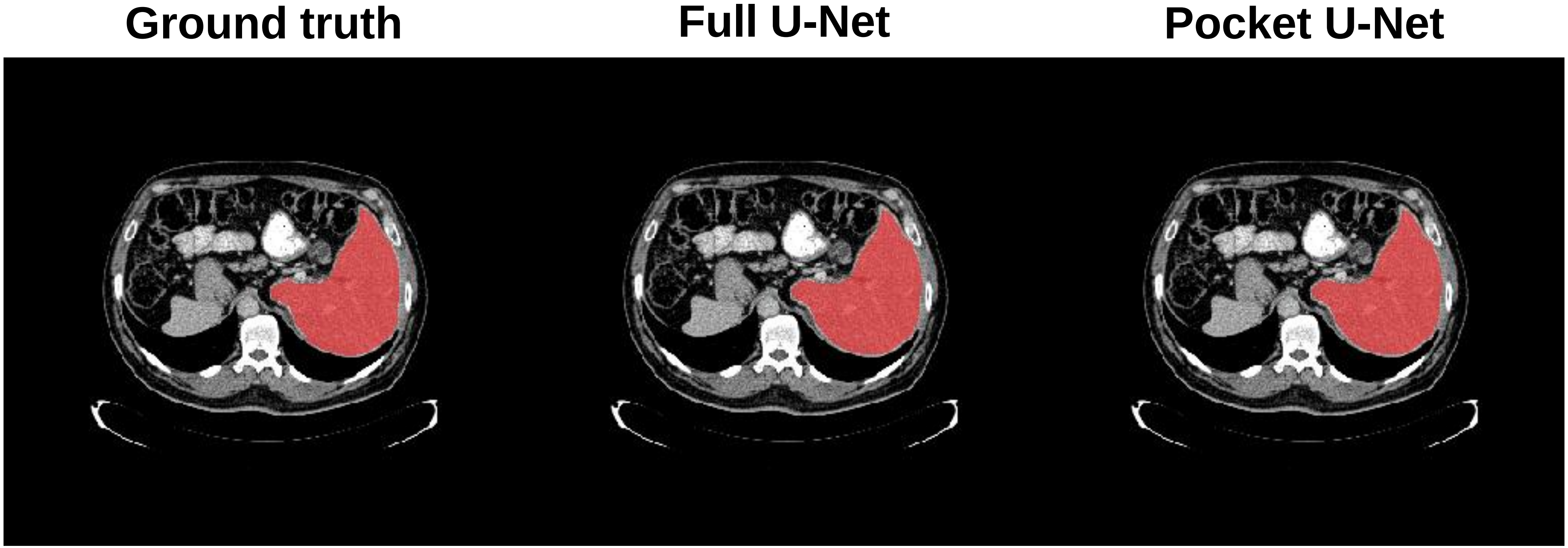

Comparable Accuracy – LiTS

Task	Architecture	Variant	# Params (M)	Hausdorff 95 (mm) Mean (Std)	Hausdorff 95 (mm) Median	p-value
LiTS	U-Net	Full	90.5	9.715 (23.95)	0.967	NS
		Pocket	0.8	7.845 (21.67)	0.959	
	ResNet	Full	91.9	9.105 (28.40)	0.729	NS
		Pocket	0.8	10.38 (26.90)	0.742	
	DenseNet	Full	135.9	18.97 (50.65)	0.781	NS
		Pocket	1.3	10.16 (27.21)	1.000	
	HRNet	Full	6.5	6.126 (19.37)	0.756	NS
		Pocket	0.7	8.805 (26.97)	0.787	
	nnUNet	Full	31.2	6.364 (12.88)	1.182	NS
		Pocket	0.8	4.086 (18.55)	0.758	

NS, $p\text{-value} > 0.05$

*, $p\text{-value} < 0.05$

**, $p\text{-value} < 0.01$

***, $p\text{-value} < 0.001$

MICCAI BraTS 2024

- MIST model has 771,000 parameters
- nnUNet has 31,000,000 parameters
- Trained five-fold cross-validation with 8 H100 GPUs for 4 days

MICCAI BraTS 2024

Class	Labels	Dice	Hausdorff 95 (mm)
NETC	1	0.7010	58.165
SNFH	2	0.9208	6.6536
ET	3	0.7427	27.950
RC	4	0.6841	49.321
TC	1, 3	0.7379	28.514
WT	1, 2, 3	0.9257	6.6367

Accuracy in terms of the Dice and 95th percentile Hausdorff distances for each segmentation class in the Adult Glioma Post-Treatment validation dataset.

Liver Segmentation Experiments

Three Models

- SMIT (Swin UNet Transformers)
- Pocketnet NNU-Net
- NNUnet-version 2

Two Experiments:

- Experiment 1: Single Origin
- Experiment 1: Multi-site Origin

Comprehensive Dataset:

- AMOS
- ATLAS
- CHAOS
- DUKE
- MDACC
- Methodist

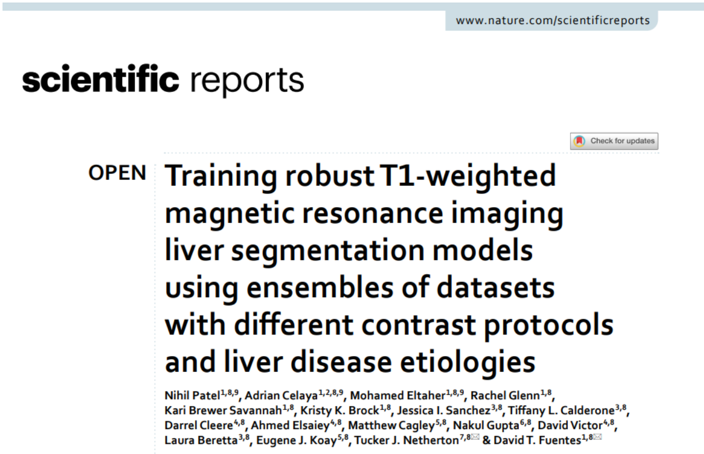
www.nature.com/scientificreports

scientific reports

Check for updates

OPEN Training robust T1-weighted magnetic resonance imaging liver segmentation models using ensembles of datasets with different contrast protocols and liver disease etiologies

Nihil Patel[1,8,9], Adrian Celaya[1,2,8,9], Mohamed Eltaher[1,8,9], Rachel Glenn[1,8], Kari Brewer Savannah[1,8], Kristy K. Brock[1,8], Jessica I. Sanchez[3,8], Tiffany L. Calderone[3,8], Darrel Cleere[4,8], Ahmed Elsaiey[4,8], Matthew Cagley[5,8], Nakul Gupta[6,8], David Victor[4,8], Laura Beretta[3,8], Eugene J. Koay[5,8], Tucker J. Netherton[7,8] & David T. Fuentes[1,8]

Comprehensive Dataset-T1 MRI data

Origin	Patients	Images	Image Distribution	
CHAOS	20	40	In phase (n=20)	Opposed Phase (n=20)
DLDS	72	210	In Phase non-Fat Saturation (n=56) Late dynamic (n=2) Opposed phase (n=36)	Precontrast Fat Suppressed (n=54) Early Arterial (n=1) Mid Arterial (n=3) Portal Venous (n=56)
AMOS	57	57		
ADACC (Morfeus Lab)	10	12	Precontrast (n=6) Post-contrast (n=3)	Dual-Echo (n=1) 5-minute (n=2)
ATLAS	58	58	VIBE (n=58)	
Methodist	72	352	3D Axial LAVA POST Delay (n=215) Axial T1 FS VIBE (n = 74)	Axial VIBE DIXON (n = 35) Axial LAVA Delay (n=20) Coronal LAVA Post Delay (n=8)
MDACC (Koay)	34	102	Pre-Contrast (n=34)	Arterial Phase (n=34) Portal Venous Phase (n=34)

Total: 831

Liver Segmentation

- Model Generalizability

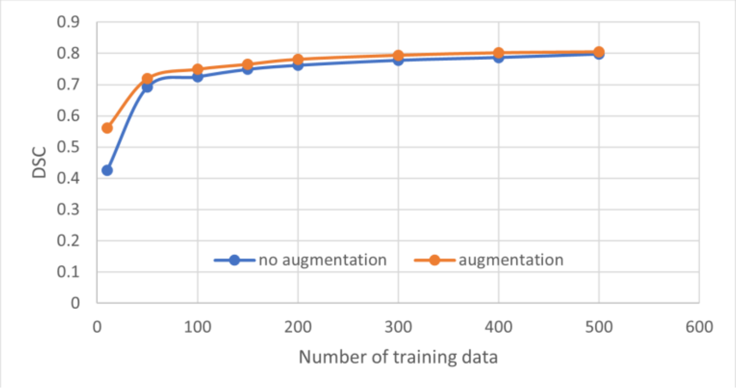

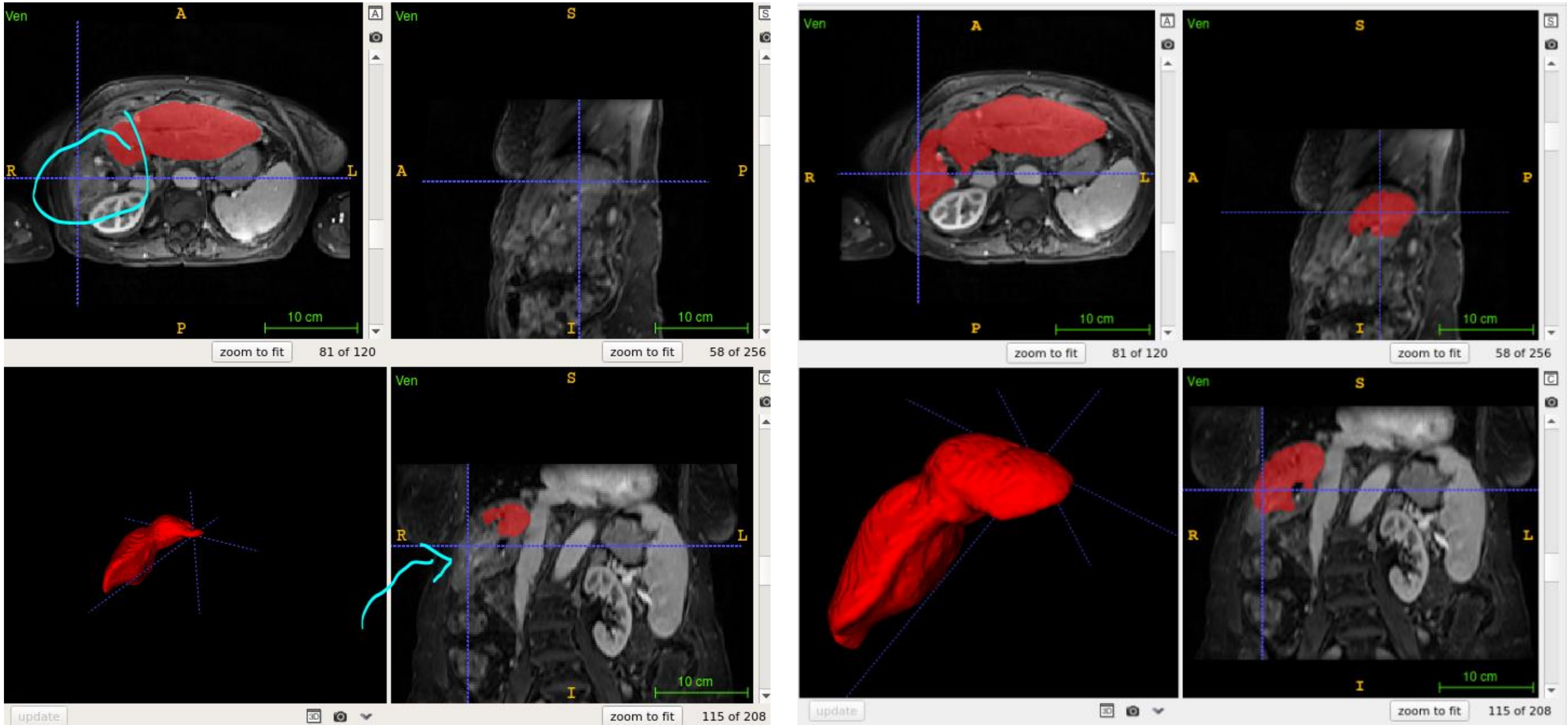

Longitudinal registration

- NN for image segmentation
- Padded liver mask reduces the optimization space of the deformable registration

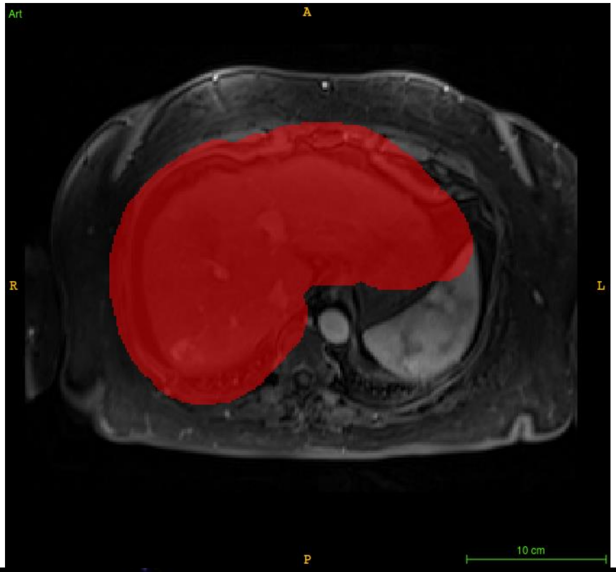

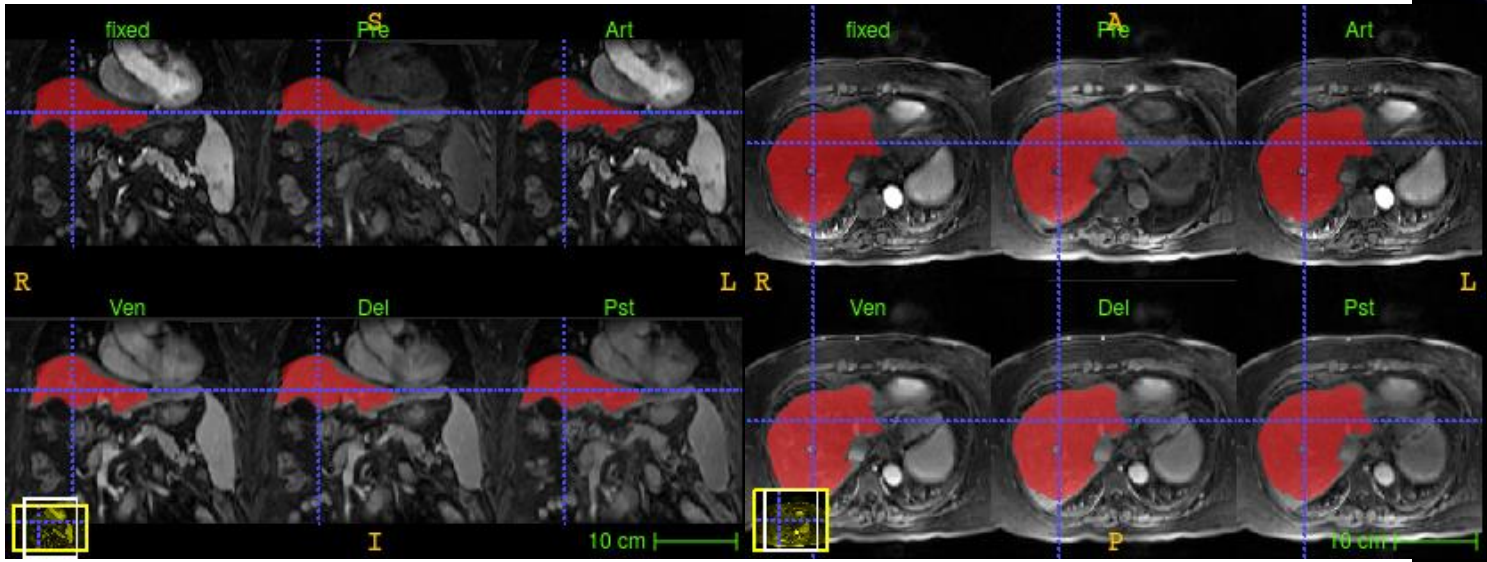

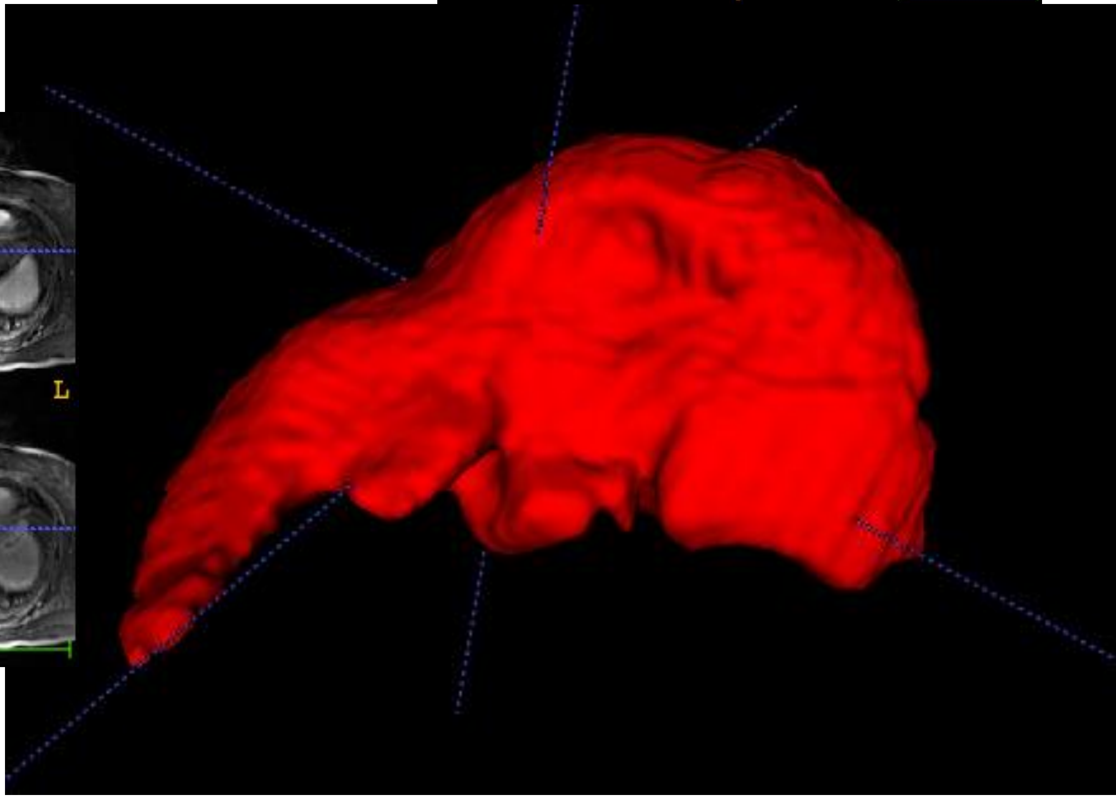

Patient Population

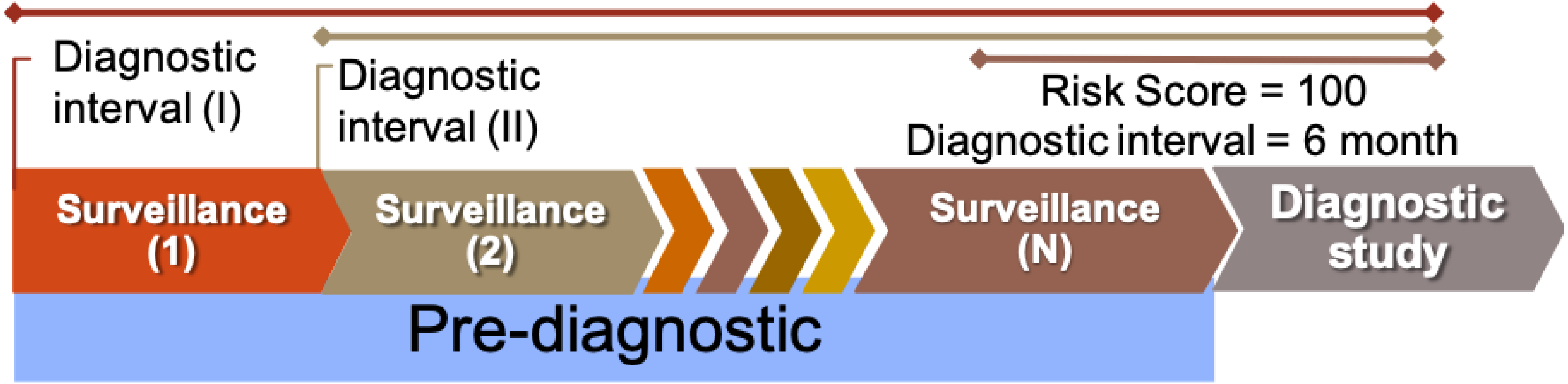

- N=48 cases, N=99 controls longitudinal data registered to the diagnostic time point (case) or baseline (control)
  - Cases = Patients with a confirmed HCC diagnosis, a diagnostic MRI, and at least one pre-diagnostic MRI
    - Hepatitis C, Alcohol, NAFLD, Hemachromatosis
  - Controls = Patients with MRI surveillance studies who don't develop HCC
    - Alcohol, NAFLD

Results

- Quantifiable differences between HCC cases and controls in a screening population with indeterminate lesions
  - The mean CNR of EPM was 3.10 vs. 2.61 on the arterial phase of the pre-diagnostic MRI and vs. 0.88 on the PV phase of MRI
- Cases - 48 patients at HCC diagnostic time point
- Control - 99 control studies
  - EPM signals of the normal liver parenchyma of the case patients and the control patients were similar

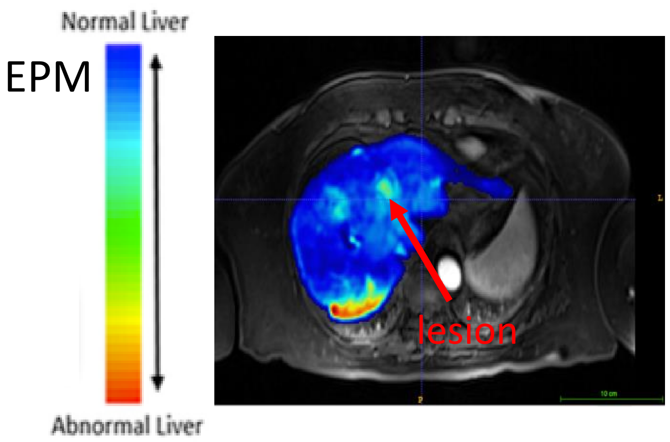

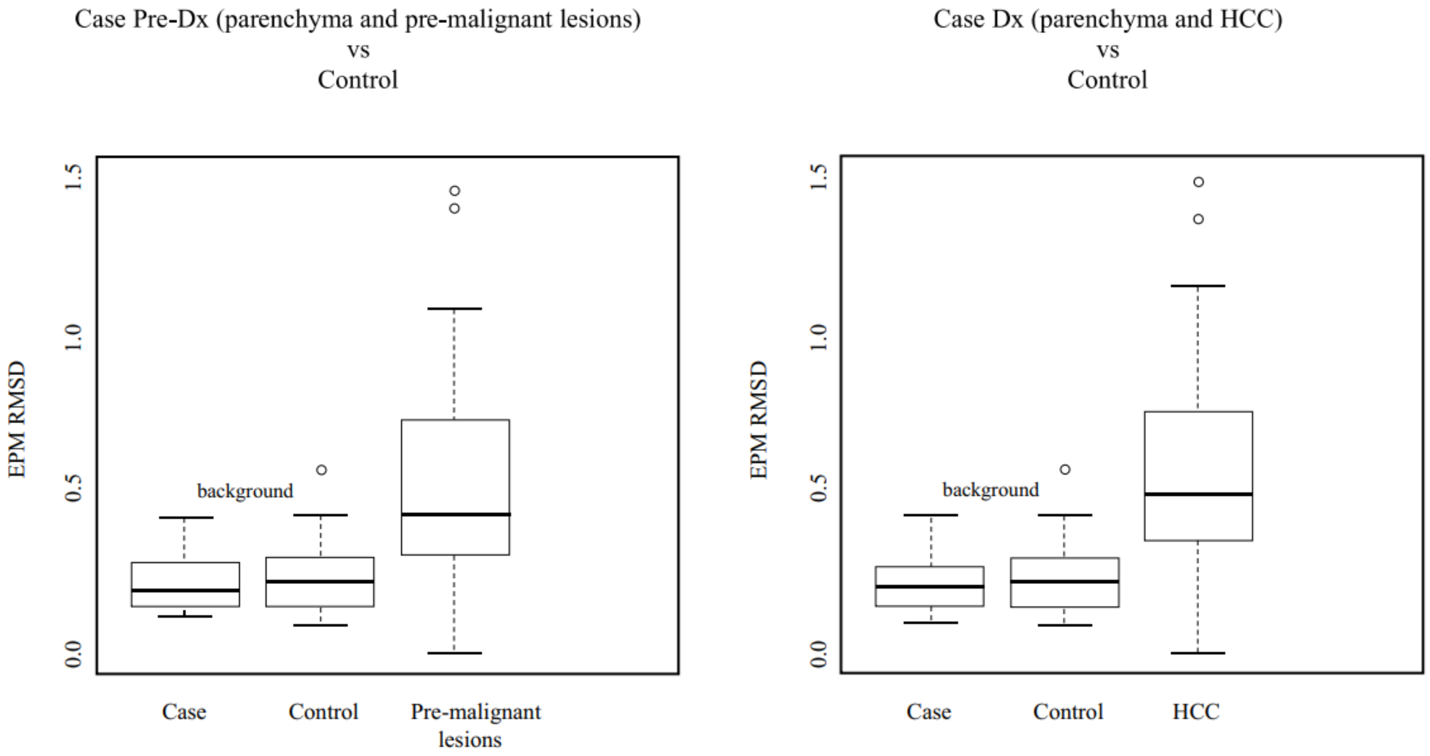

Summary

- EPM provides a unique imaging biomarker
  - EPM = .37 is our current threshold

- Work In Progress
  - Minimize Human in the Loop - Infrastructure automates the workflow to process at scale
  - Review each dataset 1-by-1 for multisite QA
    - registration failure is the typical mode of failure.

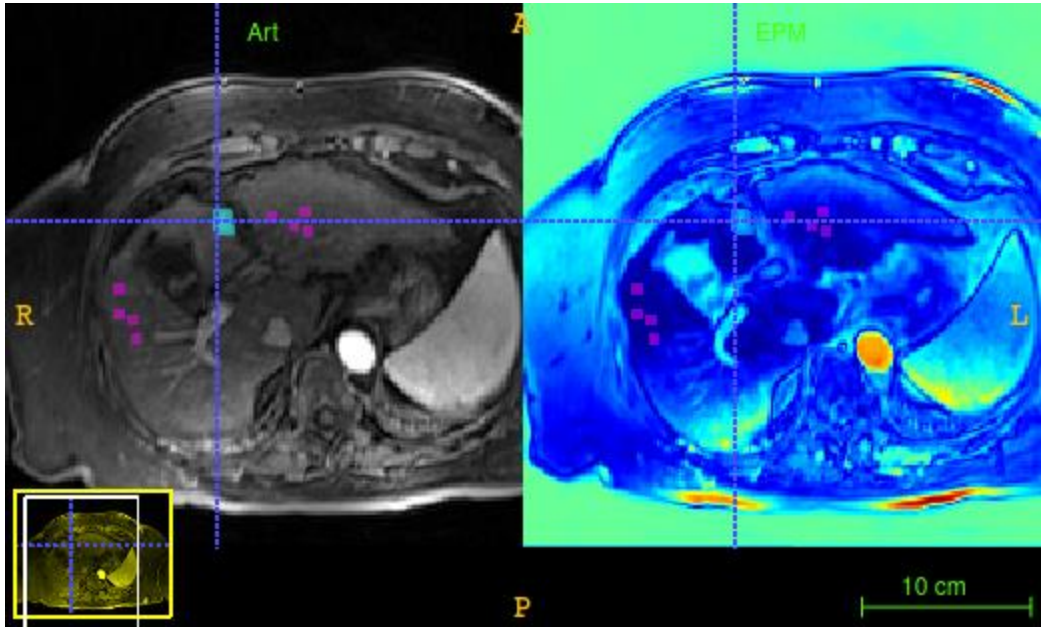

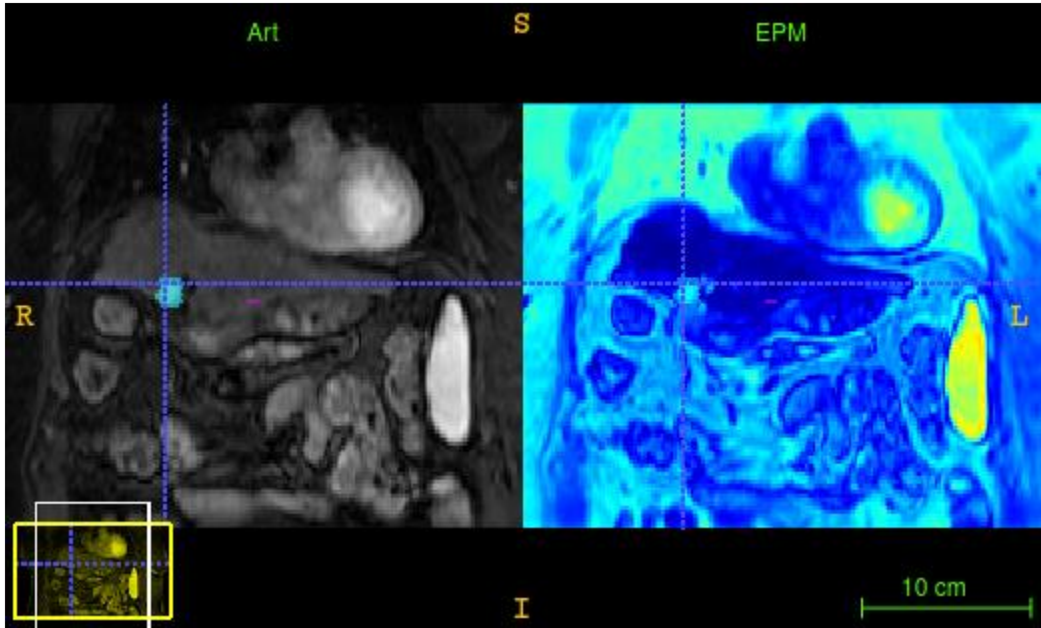

Goal

HCC probability = a * age/gender + b * blood biomarker + c * imaging biomarker

- Blood based
  - GALAD - Berhane, Toyoda, et al. 2016
  - ASAP - Yang, Xing, et al 2019.

Image based lesion classification

- Yamashita, Mittendorf et al. 2020
  - 60% accuracy LR-1/2, LR-3, LR-4, vs LR-5
- Yasaka, Akai et al. 2018
  - 84% accuracy LR-1, LR-5, vs LR-M
- Wu, White et al. 2020
  - 90% accuracy LR-3 vs LR-4/5 lesions

From: Deep convolutional neural network applied to the liver imaging reporting and data system (LI-RADS) version 2014 category classification: a pilot study

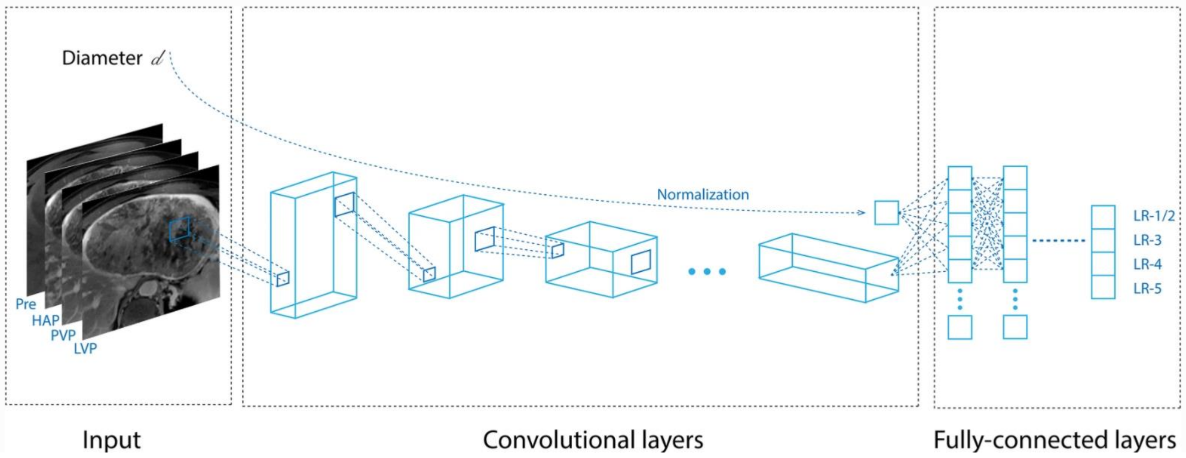

Acknowledgements

National Institutes of Health
Turning Discovery Into Health

- National Institutes of Health
  - R01CA195524, R21CA249373, U01CA230997
- Tumor Measurement Initiative
- QIAC, IRG, CCSG
- National Science Foundation
  - NSF-2111147 and NSF-2111459
- CPRIT
  - RP220119

CANCER PREVENTION & RESEARCH INSTITUTE OF TEXAS

THE UNIVERSITY OF TEXAS
MD Anderson ~~Cancer~~ Center
Making Cancer History®

Acknowledgements

- Collaborators
  - Laura Beretta
  - Ahmed Kaseb
  - Khaled Elsayes
  - Prasun Jalal
  - Manal Hassan
  - Mohamed Badawy
- Cancer Physics and Engineering Lab
  - Eugene Koay
  - Newsha Nikzad
  - Millicent Roach
  - Tasadduk Chowdhury
  - Connor Thunshelle
  - Mohamed Zaid
  - Kevin Sun

Questions ?

https://github.com/aecelaya/MIST

PocketNet…

Simple modification

Significantly reduces computational costs

Preserves accuracy

Behaves similarly to full networks under dataset size